PAPER • **OPEN ACCESS**

Highly anisotropic mechanical and optical properties of 2D NbOX2 (X = Cl, Br, I) revealed by first-principle

To cite this article: Bohayra Mortazavi *et al* 2022 *Nanotechnology* **33** 275701

OPEN ACCESS
IOP Publishing
Nanotechnology

Nanotechnology **33** (2022) 275701 (8pp)
https://doi.org/10.1088/1361-6528/ac622f

Highly anisotropic mechanical and optical properties of 2D NbOX2 (X = Cl, Br, I) revealed by first-principle

Bohayra Mortazavi[1,*], Masoud Shahrokhi[2], Brahmanandam Javvaji[1], Alexander V Shapeev[3] and Xiaoying Zhuang[1,4,*]

[1] Chair of Computational Science and Simulation Technology, Department of Mathematics and Physics, Leibniz Universität Hannover, Appelstraße 11, D-30167 Hannover, Germany
[2] Independent researcher, Lyon, France
[3] Skolkovo Institute of Science and Technology, Skolkovo Innovation Center, Bolshoy Bulvar, 30s1, Moscow, 143026, Russia
[4] College of Civil Engineering, Department of Geotechnical Engineering, Tongji University, 1239 Siping Road Shanghai, People's Republic of China

E-mail: bohayra.mortazavi@gmail.com and zhuang@iop.uni-hannover.de

Received 16 November 2021, revised 16 March 2022
Accepted for publication 29 March 2022
Published 12 April 2022

Abstract

In the latest experimental success, $NbOI_2$ two-dimensional (2D) crystals with anisotropic electronic and optical properties have been fabricated (*Adv. Mater.* 33 (2021), 2101505). In this work inspired by the aforementioned accomplishment, we conduct first-principles calculations to explore the mechanical, electronic, and optical properties of $NbOX_2$ (X = Cl, Br, I) nanosheets. We show that individual layers in these systems are weakly bonded, with exfoliation energies of 0.22, 0.23, and 0.24 J m^{-2}, for the isolation of the $NbOCl_2$, $NbOBr_2$, and $NbOI_2$ monolayers, respectively, distinctly lower than those of the graphene. The optoelectronic properties of the single-layer, bilayer, and bulk $NbOCl_2$, $NbOBr_2$, and $NbOI_2$ crystals are investigated via density functional theory calculations with the HSE06 approach. Our results indicate that the layered bulk $NbOCl_2$, $NbOBr_2$, and $NbOI_2$ crystals are indirect gap semiconductors, with band gaps of 1.79, 1.69, and 1.60 eV, respectively. We found a slight increase in the electronic gap for the monolayer and bilayer systems due to electron confinement at the nanoscale. Our results show that the monolayer and bilayer of these novel 2D compounds show suitable valence and conduction band edge positions for visible-light-driven water splitting reactions. The first absorption peaks of these novel monolayers along the in-plane polarization are located in the visible range of light which can be a promising feature to design advanced nanoelectronics. We found that the studied 2D systems exhibit highly anisotropic mechanical and optical properties. The presented first-principles results provide a comprehensive vision about direction-dependent mechanical and optical properties of $NbOX_2$ (X = Cl, Br, I) nanosheets.

Supplementary material for this article is available online

Keywords: 2D $NbOI_2$, anisotropic, optical, mechanical, semiconductor, photocatalysis

(Some figures may appear in colour only in the online journal)

* Authors to whom any correspondence should be addressed.

1. Introduction

Graphene [1–3], the frontier member of the two-dimensional (2D) materials family with a planar and honeycomb full-carbon lattice, exhibits exceptional mechanical [4], heat transport [5, 6], and electronic properties [7–10]. The zero-gap electronic nature of pristine graphene limits its effectiveness for numerous cutting-edge technologies. This drawback motivated the prediction and synthesis of novel 2D inherent semiconductors, such as: graphitic C_3N_4 [11], transition metal dichalcogenides [12–14], germanium arsenide [15], phosphorene [16, 17], $MoSi_2N_4$ [18], penta-PdPSe [19] and most recently nickel diazenide NiN_2 [20] nanosheets. As the continuous trend of the expansion of experimentally realized 2D semiconductors, most recently Fang *et al* [21] succeeded in the growth of $NbOI_2$ 2D crystals. They employed a chemical vapor transport method to fabricate high-quality $NbOI_2$ nanosheets. Their experimental measurements confirm that this novel 2D system exhibits angle-dependent electronic and optoelectronic properties. This experimental advance may provide a possibility for the synthesis of the $NbOCl_2$ and $NbOBr_2$ counterparts. In this work, our objective is to theoretically examine the critical physical properties of the $NbOCl_2$, $NbOBr_2$, and $NbOI_2$ 2D lattices. For this purpose, we conduct density functional theory (DFT) calculations to examine the exfoliation energy, mechanical, electronic, optical, and photocatalytic properties of the $NbOCl_2$, $NbOBr_2$, and $NbOI_2$ nanosheets. We particularly examine the thickness effect on the optoelectronic properties of these novel 2D lattices. The presented first-principles results by this study confirm the outstanding mechanical properties and offer a comprehensive vision on the direction-dependent physical properties of $NbOCl_2$, $NbOBr_2$, and $NbOI_2$ nanosheets and highlight their prospect to design next-generation anisotropic optoelectronic and energy conversion nanodevices.

2. Computational methods

First-principles DFT calculations are performed by employing the *Vienna Ab initio Simulation Package* [22, 23]. The generalized gradient approximation (GGA) was adopted with the Perdew–Burke–Ernzerhof (PBE) exchange-correlation functional. The plane wave cutoff energy and self-consistent loop cutoff energy are set to 500 and 10^{-5} eV, respectively. To obtain the geometry-optimized and stress-free structures, atomic positions and lattice sizes are relaxed using conjugate gradient algorithm until Hellman–Feynman forces drop below 0.001 eV Å [24] with the $11 \times 11 \times 1$ Monkhorst–Pack [25] K-point grid. Periodic boundary conditions are considered in all the directions and in order to avoid interactions with systems' periodic images along the nanosheets' thickness the size of the cell was set to 20 and 25 Å for the monolayer and bilayer structures, respectively. For the multilayered structures, we also adopt the DFT-D3 [26] dispersion correction by Grimme to better count for van der Waals interactions. The electronic properties are analyzed by employing the PBE/GGA and HSE06 hybrid [27] functional. We utilize a Γ-centered k-point grid of $8 \times 16 \times 1$ to evaluate the electronic properties of the monolayer and bilayer structures. In the evaluation of the optical properties with the random phase approximation (RPA) approach, a denser k-point mesh size of $16 \times 32 \times 1$ was used. For the analysis of the electronic and optical properties of bulk structures, we use $8 \times 16 \times 6$ and $16 \times 32 \times 12$ k-points, respectively. For optical properties calculations for the monolayer and bilayer structures a lattice size of 45 Å is applied along sheets' normal direction [28]. For the analysis of optical properties only the electronic contributions to the frequency dependent dielectric function were considered and the ionic contributions to the frequency dependent dielectric function were not taken into account. For more details about calculations of optical properties, refer to the supplementary information document (available online at stacks.iop.org/NANO/33/275701/mmedia).

3. Results and discussions

We first study the structural properties and bonding mechanism of the $NbOCl_2$, $NbOBr_2$, and $NbOI_2$ monolayers and their bulk counterparts. It is worthwhile to mention that according to our spin-polarized calculations, these systems at their ground state are found to be nonmagnetic. As the representative structure, in figure 1, the geometry-optimized (a)–(c) single-layer and (d) bulk $NbOCl_2$ lattices along with the isosurface and section maps of electron localization function (ELF) [29] are illustrated. In order to investigate the anisotropicity in the mechanical and optical response, we consider two different directions of x and y as distinguished in figure 1. The energy-minimized and stress-free monolayer, bilayer, and bulk $NbOX_2$ (X = Cl, Br, I) lattices are included in the supplementary information document. Generally, we found a close agreement between our predicted structural parameters with experimental values for bulk lattices (find table S1). According to the Bader charge analysis [30], we found that Nb atoms, on average, tend to transfer 2.19, 2.05, and 1.86 e to the surrounding atoms in the $NbOCl_2$, $NbOBr_2$, and $NbOI_2$ monolayers, respectively. This is an expectable finding, knowing that the electronegativity of Nb is much smaller than other atoms in these systems. Interestingly, almost irrespective of the halogen atom types, O atoms tend to gain around 1.1 e from Nb atoms. It is worthwhile to note that ELF is a spatial function defined between 0 and 1, and ELF values close to unity reveal strong covalent interaction or lone pair electrons, whereas lower ELF values represent weaker ionic, metallic, or van der Waals interactions. As shown in figure 1(f), the ELF contour around the center of Nb-halogen bonds approaches zero, revealing ionic interaction governance. A similar finding but with lower intensity is also consistent for the Nb–O bonds, also revealing the prevalence of the ionic bonding alongside with low contribution of covalent bonding. These results suggest the dominance of ionic bonding in these novel 2D systems.

After analyzing the bonding mechanism of $NbOX_2$ (X = Cl, Br, I) lattices, we next study their mechanical features. In this regard, the uniaxial stress–strain responses of the

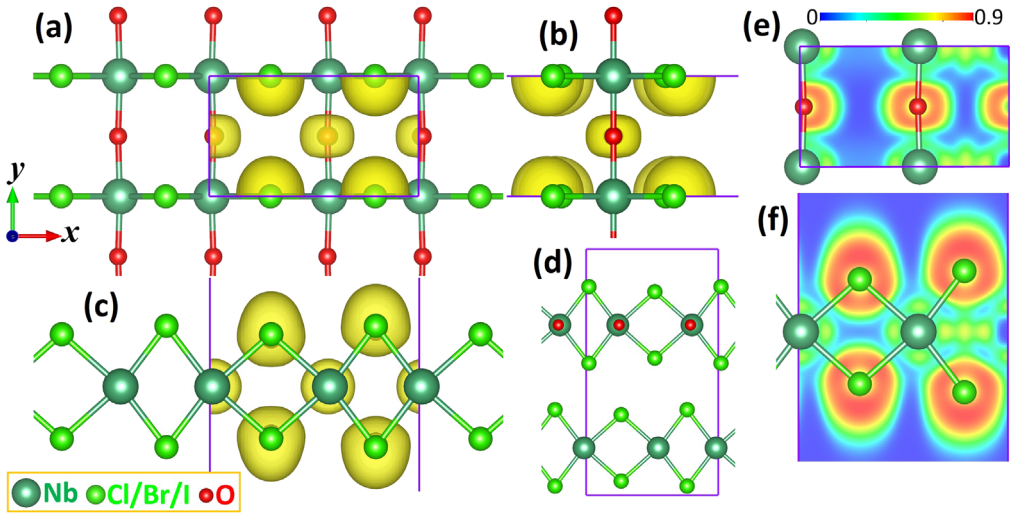

Figure 1. (a) Top and (b), (c) side views of the $NbOCl_2$ monolayer along with electron localization function (ELF) isosurface set to 0.7. (d) Side view of the bulk $NbOI_2$. ELF sections for the (e) top and (f) side view of the $NbOCl_2$ monolayer.

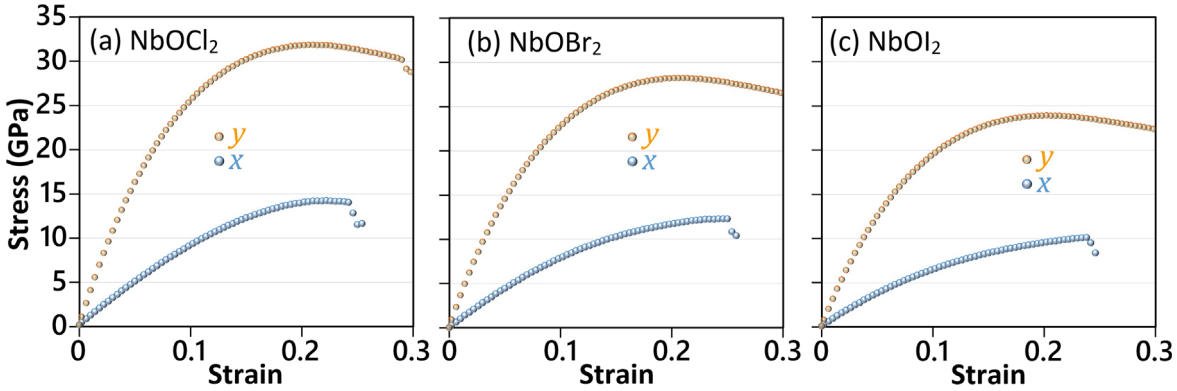

Figure 2. True uniaxial stress–strain relations of the (a) $NbOCl_2$, (b) $NbOBr_2$, and (c) $NbOI_2$ monolayers elongated along the *y* and *x* directions.

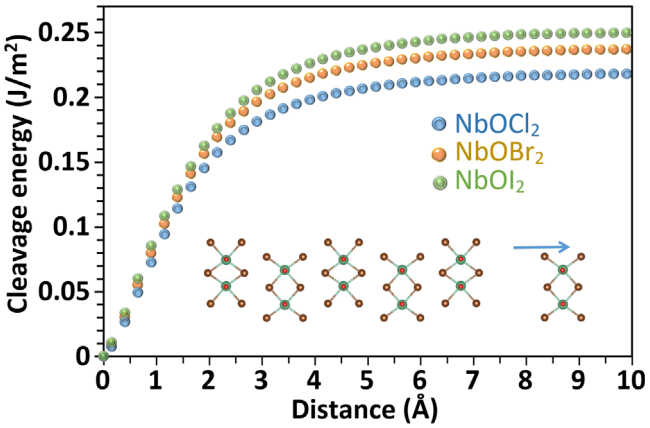

Figure 3. Estimated cleavage energy of the $NbOCl_2$, $NbOBr_2$, and $NbOI_2$ monolayers from their six-layered structures as a function of separation distance.

$NbOX_2$ monolayers along the *x* and *y* directions are illustrated in figure 2. The presented stress–strain curves are in the standard GPa unit and are thus based on the actual volume of the deformed monolayers [31, 32]. The area of the monolayers can be simply obtained using the simulation-box sizes along the planar directions. The thickness at every step is calculated as the normal distance between boundary halogen atoms plus their effective van der Waals diameter (vdW). In this regard, according to our geometry optimization results of the bulk structures, the thickness of the $NbOCl_2$, $NbOBr_2$, and $NbOI_2$ monolayers is calculated to be 6.281, 6.772, 7.456 Å, respectively, very close to the corresponding experimentally reported values of 6.395 [33], 6.898 [34] and 7.518 [35] Å, respectively. With the conducted geometry optimizations, we measured 3.929, 4.234, and 4.613 Å distances between boundary halogen atoms in the $NbOCl_2$, $NbOBr_2$, and $NbOI_2$ monolayers, respectively, which are in correspondence with effective vdW diameters of 2.351, 2.539, and 2.843 Å, for Cl, Br and I atoms, respectively, in these systems. In addition, the stress–strain curves in figure 2 are uniaxial, which means that during the deformation, the structures are stressed only along the loading direction and are stress-free along the two other perpendicular directions of the loading. Since we investigate the mechanical properties of monolayers that are not constrained along their thickness direction, upon the geometry minimization, the system's stress component normal along

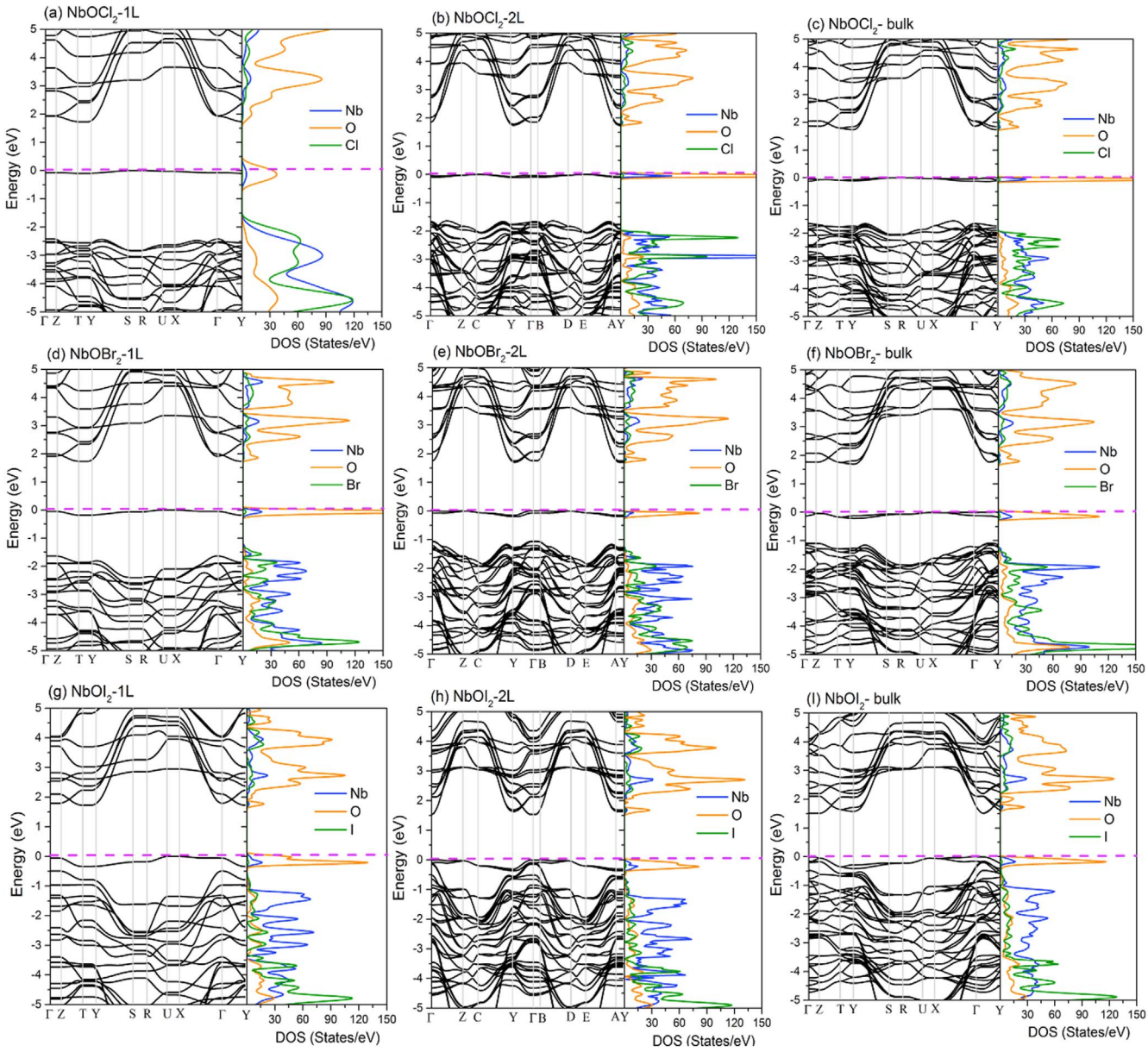

Figure 4. Electronic band structure and partial electronic density of states PDOS for the monolayer (1L), bilayer (2L), and bulk structure of $NbOCl_2$, $NbOBr_2$, and $NbOI_2$ compounds. The purple dashed lines indicate the Fermi energy.

this direction reaches a negligible value. Therefore, in the conducted DFT simulations, the simulation cell size along the other in-plane perpendicular direction of the loading (either *x* or *y*) is adjusted to satisfy the negligible stress condition after the geometry minimization.

From the predicted uniaxial true stress–strain responses of the $NbOX_2$ monolayers illustrated in figure 2, remarkable differences for the loading along the *x* and *y* directions are conspicuous, confirming the highly anisotropic and direction-dependent mechanical responses in these systems. The elastic modulus of the $NbOCl_2$, $NbOBr_2$, and $NbOI_2$ monolayers along the *y* (*x*) directions are predicted to be 390 (111), 354 (95), and 314(84) GPa, respectively. In contrast to the observed substantial role of halogen atom on the elastic modulus, Poisson's ratio values of these monolayers are found to be close, with corresponding values of 0.04 (0.01), 0.03 (0.01), and 0.03 (0.01), respectively, for the $NbOCl_2$, $NbOBr_2$, and $NbOI_2$ monolayers along the *y* (*x*) directions. The ultimate tensile strength of the $NbOCl_2$, $NbOBr_2$, and $NbOI_2$ monolayers along the *y* (*x*) directions are predicted to be 31.8(14.2), 28.2 (14.2), and 23.9 (11.4) GPa, respectively. These results reveal that these nanosheets are remarkably stronger along the *y* direction than *x* direction. Moreover, clear decreasing trends in the elastic modulus and tensile strengths of the $NbOX_2$ monolayers with the increase of the atomic weight of halogen atoms are observable. The anisotropic mechanical responses in these 2D systems can be easily explained by considering their atomic structure. We know that the orientation of different bonds along the loading direction plays a critical role in the load transfer. For the loading along the *y* direction, Nb–O bonds are directly oriented along the loading direction, and the deformation can

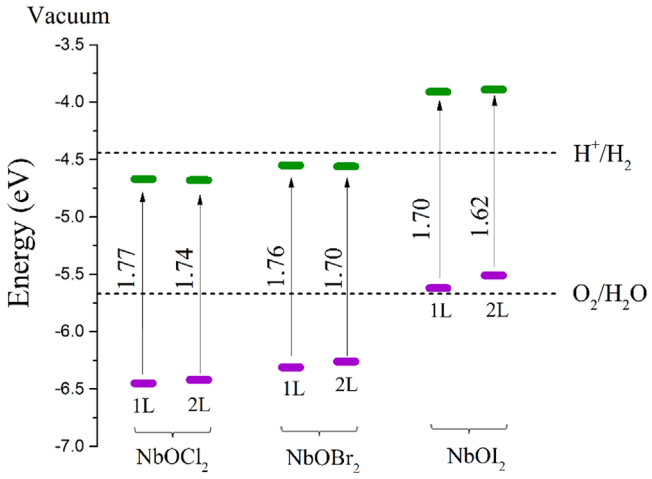

Figure 5. Calculated conduction (green color) and valence band (purple color) edge positions for the monolayer (1L) and bilayer (2L) $NbOCl_2$, $NbOBr_2$, and $NbOI_2$ compounds with respect to the vacuum level. The dashed black lines indicate the water stability limits for hydrogen and oxygen evolution. The absolute potential of the standard hydrogen electrode was taken as 4.44 eV at a pH = 0.

Table 1. The HSE06 electronic band gap (E_g) and static dielectric constant for the monolayer (1L) and bilayer (2L) and bulk structures of $NbOCl_2$, $NbOBr_2$, and $NbOI_2$ compounds.

System	Band gap (eV)	Static dielectric constant $E\|\|xE\|\|yE\|\|z$
$NbOCl_2$		
1L	1.77	2.50 2.14 1.80
2L	1.74	3.30 2.67 2.17
Bulk	1.72	5.80 4.51 3.58
$NbOBr_2$		
1L	1.76	2.82 2.29 2.08
2L	1.70	3.77 2.86 2.64
Bulk	1.69	6.33 4.67 4.31
$NbOI_2$		
1L	1.70	3.48 2.72 2.61
2L	1.62	4.74 3.44 3.50
Bulk	1.60	7.56 5.41 5.62

proceed only by the direct elongation of these bonds. In contrast, for the loading along the *x* direction, the deformation is achieved by a mixture of Nb–X bond elongation and Nb–X–Nb angle opening. In other words, along the *x* direction the halogen atoms yield a pivot-like behavior, facilitating the deformation and consequently resulting in a lower elastic modulus and tensile strength. As an example, for the $NbOCl_2$ monolayer under the strain of 0.2, the reduction of the monolayer's thickness along the *x* and *y* directions is predicted to be around 6.3 and 0.9%, respectively, revealing a contrasting deformation mechanism.

Before exploring the electronic and optical properties of $NbOX_2$ nanosheets, we investigate the required energy for the isolation of the $NbOCl_2$, $NbOBr_2$, and $NbOI_2$ monolayers from their multilayered counterparts. To this end, we simulate the exfoliation process and predict the corresponding cleavage energy, as illustrated in figure 3. In these calculations, after the geometry optimization of six-layered structures, the last layer was gradually separated toward the vacuum with a 0.25 Å step, and the change in the systems' energy was recorded. As expected, the exfoliation energy first increases sharply and subsequently at separation distances around 6 Å reaches a plateau and later completely converges. It is predicted that individual layers in these systems are weakly bonded, with exfoliation energies of 0.22, 0.23, and 0.24 J m^{-2}, for the $NbOCl_2$, $NbOBr_2$, and $NbOI_2$ monolayers, respectively, which are distinctly lower than the measured cleavage energy of 0.37 J m^{-2} for graphite [36]. A slight increasing trend in the exfoliation energy with the increase of the atomic weight of halogen atoms is observable. These results reveal the bright practical prospect for isolating the $NbOCl_2$, $NbOBr_2$, and $NbOI_2$ monolayers from their bulk counterparts.

We next study the electronic and optical properties of these systems. To probe the electronic properties of the studied compounds, the band structures along the high symmetry directions and the partial density of states (PDOS) of these systems were calculated within the HSE06 approach, as shown in figure 4. Moreover, the valence band (VB) and conduction band (CB) edge positions of these systems have been calculated using HSE06 and shown in figure 5. The obtained electronic band structures reveal that the considered nanosheets possess an indirect electronic band gap. The band gap values for each structure are also summarized in table 1. The electronic band gap of $NbOCl_2$, $NbOBr_2$ and $NbOI_2$ bulk structures are predicted here to be 1.72, 1.69 and 1.60 eV, respectively, which present a good agreement with the reported experimental optical band gap value of 1.75 eV for $NbOI_2$ in [21]. Our results show that the band gap of these layered structures is relatively constant (table 1) as the number of layers increases from single-layer (1L) to bulk. The electronic band gap of $NbOCl_2$, $NbOBr_2$ and $NbOI_2$ monolayers obtained with HSE06 approach is 1.77, 1.76 and 1.70 eV, respectively, which are generally in good agreement with the previous theoretical work [33] using the same technique. Nevertheless, the obtained band gap values for few-layered structures using HSE06 are still smaller than experimental values. Such a discrepancy can be attributed to the effects of defects or impurities in experimental tests or might be associated with the accuracy of HSE06 approach, which can be improved using quasi-particle GW calculations, highly interesting to be assessed in a separate study. The PDOS of these layered structures indicates that both the top of the valence band and the bottom of the conduction band are dominated by O 2p states with hybridization of Nb 4d orbitals. Moreover, the VB and CB edges in each layered system remain almost unchanged, which confirms the pure vdW interactions between the layers. The VB and CB edge positions overall shift to lower potential with the increase of the atomic number of the halogen elements Cl, Br, and I. It can be seen that the $NbOCl_2$ and $NbOBr_2$ nanosheet are predicted to be good candidates only for the water oxidation and O_2 evolution, while the $NbOI_2$ counterpart can be used only for hydrogen evolution.

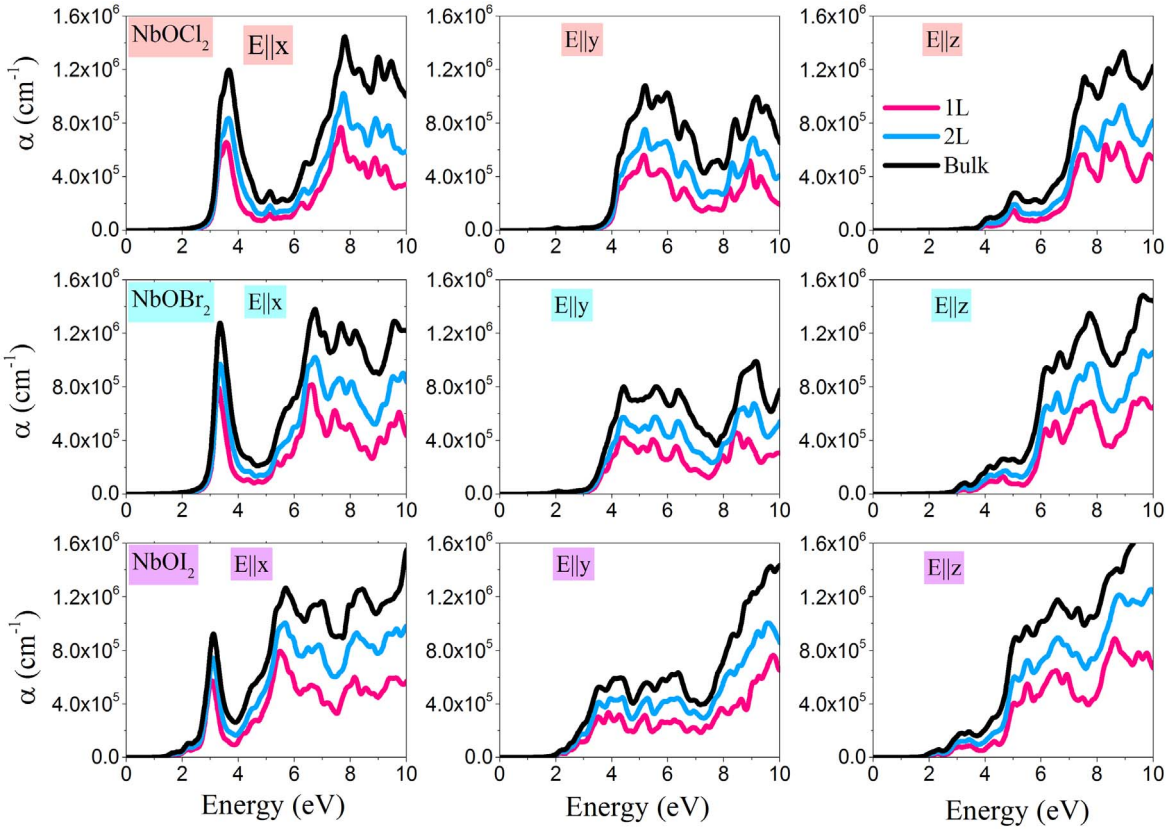

Figure 6. Optical absorption spectra α as a function of energy predicted using the RPA + HSE06 approach for the monolayer (1L) and bilayer (2L) and bulk $NbOCl_2$, $NbOBr_2$ and $NbOI_2$ compounds to the in-plane (*x*- and *y*-polarized) and out-of-plane (*z*-polarized) incident light.

We next discuss the optical responses of the monolayer, bilayer, and bulk $NbOCl_2$, $NbOBr_2$, and $NbOI_2$ compounds using the RPA method constructed over HSE06. Because of the asymmetric geometry along the *x*-, *y*- and *z*-axes, the optical spectra of these structures are anisotropic for light polarizations along the in-plane and out-of-plane directions. Hence, the optical properties for the both *x*-, *y*- and *z*-polarized direction ($E||x$, $E||y$ and $E||z$) are reported. The imaginary and real parts of the dielectric function (Im ε and Re ε) of the $NbOCl_2$, $NbOBr_2$, and $NbOI_2$ compounds for the in-plane and out-of-plane polarized directions versus photon energy were calculated, and the obtained results are illustrated in figures S1, S2, and S3 (see the supplementary information document), respectively. The absorption edges of Im ε of these materials occur at an energy range between ∼2.0 and 4.0 eV along different polarizations in the visible range of light. In all of these structures, the absorption edge of Im ε shift to the lower energies as the number of layers increases from the monolayer to bulk. It can also be seen that the absorption edge of the Im ε overall shifts to lower energy with the increase of the atomic number of halogen elements. The values of the static dielectric constant (the values of Re ε at zero energy) for these novel layered structures are reported in table 1. In general, in all these systems, the static dielectric constant increases with the number of layers from the monolayer to bulk. Moreover, there is an increase in the static dielectric constant values with the increase of the atomic number of Cl, Br, and I halogen elements.

The absorption coefficient α for these novel layered materials along the in-plane and out-of-plane polarization as a function of photon energy is plotted in figure 6. The absorption edge of α for all structures occurs at the photon energy range between 2 and 4 eV along the *x* direction, which is in the visible-light range, while the corresponding absorption edge along *y*- and *z*-axes shifts to the higher energies (blue shift). In general, contrary to the indirect band gap nature of the studied novel layered materials, the high absorption coefficients in the visible range of light are attained ($\sim 10^5$ cm^{-1}) for all structures which are higher than the typical absorption coefficient value for direct band gap semiconductors [37]. Moreover, the results of anisotropic optical properties along the in-plane directions for the studied novel monolayers suggest that they exhibit attractive prospects for the design of novel electronic and optical nanodevices that exploit their anisotropic properties, such as polarization-sensitive photodetectors.

4. Concluding remarks

Motivated by the latest report concerning the synthesis of 2D $NbOI_2$ crystals [21] using the chemical vapor transport method, we herein conduct extensive first-principles

calculations to explore the physical properties of the $NbOX_2$ (X = Cl, Br, I) nanosheets. It is shown that individual layers in these systems are weakly bonded, with single-layer exfoliation energies of 0.22, 0.23, and 0.24 J m^{-2}, for NbOCl2, $NbOBr_2$, and $NbOI_2$ crystals, respectively, distinctly lower than that of graphite. Uniaxial stress–strain results highlight the highly anisotropic mechanical characteristics of these novel 2D systems. The elastic modulus of the $NbOCl_2$, $NbOBr_2$, and $NbOI_2$ monolayers along the *y* (*x*) directions are predicted to be 390 (111), 354 (95), and 314 (84) GPa, respectively, with the corresponding ultimate tensile strength of 31.8 (14.2), 28.2 (14.2) and 23.9 (11.4) GPa, respectively. Anisotropic mechanical responses in these systems are attributed to the very different bonding configurations along the two planar directions. It is shown that the 3D and 2D structures of the $NbOCl_2$, $NbOBr_2$, and $NbOI_2$ compounds are indirect band gap semiconductors according to the HSE06 method results. Moreover, the evaluation of VB and CB edge positions confirms that the monolayer and bilayer $NbOX_2$ structures possess suitable band edge positions for photocatalytic water splitting reactions. Finally, the linear photon energy-dependent dielectric functions of the considered materials are investigated with the RPA + HSE06 approach. The optical analysis indicates that the optical spectra for these materials are anisotropic to the in-plane and out-of-plane incident light. It is also found that the first absorption peaks of these structures are located in the visible range of light. These results show that these novel materials might be appealing for optoelectronic devices, such as polarization-sensitive photodetectors and photocatalytic applications. The obtained results provide an extensive vision concerning the direct-dependent physical properties of the $NbOX_2$ nanosheets and may serve as a valuable guide for further theoretical and experimental studies on these attractive 2D systems.

Acknowledgments

B M and X Z appreciate the funding by the Deutsche Forschungsgemeinschaft (DFG, German Research Foundation) under Germany's Excellence Strategy within the Cluster of Excellence PhoenixD (EXC 2122, Project ID 390833453). The authors also acknowledge the support of the cluster system team at the Leibniz Universität of Hannover. B M is greatly thankful to the VEGAS cluster at Bauhaus University of Weimar for providing the computational resources. A V S is supported by the Russian Science Foundation (Grant No 18-13-00479, https://rscf.ru/project/18–13–00479/).

Data availability statement

All data that support the findings of this study are included within the article (and any supplementary files).

ORCID iDs

Bohayra Mortazavi https://orcid.org/0000-0003-3031-5057
Masoud Shahrokhi https://orcid.org/0000-0003-3656-6551

References

[1] Novoselov K S, Geim A K, Morozov S V, Jiang D, Zhang Y, Dubonos S V, Grigorieva I V and Firsov A A 2004 Electric field effect in atomically thin carbon films *Science* **306** 666–9
[2] Geim A K and Novoselov K S 2007 The rise of graphene *Nat. Mater.* **6** 183–91
[3] Castro Neto A H, Peres N M R, Novoselov K S, Geim A K and Guinea F 2009 The electronic properties of graphene *Rev. Mod. Phys.* **81** 109–62
[4] Lee C, Wei X, Kysar J W and Hone J 2008 Measurement of the elastic properties and intrinsic strength of monolayer graphene *Science* **321** 385–8
[5] Ghosh S, Calizo I, Teweldebrhan D, Pokatilov E P, Nika D L, Balandin A A, Bao W, Miao F and Lau C N 2008 Extremely high thermal conductivity of graphene: prospects for thermal management applications in nanoelectronic circuits *Appl. Phys. Lett.* **92** 2907977
[6] Balandin A A, Ghosh S, Bao W, Calizo I, Teweldebrhan D, Miao F and Lau C N 2008 Superior thermal conductivity of single-layer graphene *Nano Lett.* **8** 902–7
[7] Berger C *et al* 2004 Ultrathin epitaxial graphite; 2d electron gas properties and a route toward graphene-based nanoelectronics *J. Phys. Chem. B* **108** 19912–6
[8] Liu M, Yin X, Ulin-Avila E, Geng B, Zentgraf T, Ju L, Wang F and Zhang X 2011 A graphene-based broadband optical modulator *Nature* **474** 64–7
[9] Withers F, Dubois M and Savchenko A K 2010 Electron properties of fluorinated single-layer graphene transistors *Phys. Rev. B* **82** 073403
[10] Liu B and Zhou K 2019 Recent progress on graphene-analogous 2D nanomaterials: properties, modeling and applications *Prog. Mater Sci.* **100** 99–169
[11] Algara-Siller G *et al* 2014 Triazine-based graphitic carbon nitride: a two-dimensional semiconductor *Angew. Chemie-Int. Ed.* **53** 7450–5
[12] Geim A K, Grigorieva I V and Der Van 2013 Waals heterostructures *Nature* **499** 419–25
[13] Wang Q H, Kalantar-Zadeh K, Kis A, Coleman J N and Strano M S 2012 Electronics and optoelectronics of two-dimensional transition metal dichalcogenides *Nat. Nanotechnol.* **7** 699–712
[14] Radisavljevic B, Radenovic A, Brivio J, Giacometti V and Kis A 2011 Single-layer MoS_2 transistors. *Nat. Nanotechnol.* **6** 147–50
[15] Shengxue Y, Yanhan Y, Minghui W, Chunguang H, Wanfu S, Yongji G, Li H, Chengbao J, Yongzhe Z and M A P 2018 Highly in-plane optical and electrical anisotropy of 2D germanium arsenide *Adv. Funct. Mater.* **0** 1707379
[16] Das S, Demarteau M and Roelofs A 2014 Ambipolar phosphorene field effect transistor *ACS Nano* **8** 11730–8
[17] Li L, Yu Y, Ye G J, Ge Q, Ou X, Wu H, Feng D, Chen X H and Zhang Y 2014 Black phosphorus field-effect transistors *Nat. Nanotechnol.* **9** 372–7
[18] Hong Y-L *et al* 2020 Chemical vapor deposition of layered two-dimensional $MoSi_2N_4$ materials *Science* **369** 670–4

[19] Li P *et al* 2021 Penta-PdPSe: a new 2D pentagonal material with highly in-plane optical, electronic, and optoelectronic anisotropy *Adv. Mater.* **33** 2102541
[20] Bykov M *et al* 2021 Realization of an ideal cairo tessellation in nickel diazenide NiN_2: high-pressure route to pentagonal 2D materials *ACS Nano* **15** 13539–46
[21] Fang Y, Wang F, Wang R, Zhai T and Huang F 2021 2D $NbOI_2$: a chiral semiconductor with highly in-plane anisotropic electrical and optical properties *Adv. Mater.* **33** 2101505
[22] Kresse G and Furthmüller J 1996 Efficient iterative schemes for *ab initio* total-energy calculations using a plane-wave basis set *Phys. Rev. B* **54** 11169–86
[23] Perdew J P, Burke K and Ernzerhof M 1996 Generalized gradient approximation made simple *Phys. Rev. Lett.* **77** 3865–8
[24] Kresse G and Hafner J 1993 *Ab initio* molecular dynamics for liquid metals *Phys. Rev. B* **47** 558–61
[25] Monkhorst H and Pack J 1976 Special points for Brillouin zone integrations *Phys. Rev. B* **13** 5188–92
[26] Grimme S, Antony J, Ehrlich S and Krieg H 2010 A consistent and accurate *ab initio* parametrization of density functional dispersion correction (DFT-D) for the 94 elements H-Pu *J. Chem. Phys.* **132** 154104
[27] Krukau A V, Vydrov O A, Izmaylov A F and Scuseria G E 2006 Influence of the exchange screening parameter on the performance of screened hybrid functionals *J. Chem. Phys.* **125** 224106
[28] Matthes L, Pulci O and Bechstedt F 2016 Influence of out-of-plane response on optical properties of two-dimensional materials: first principles approach *Phys. Rev. B* **94** 205408
[29] Silvi B and Savin A 1994 Classification of chemical-bonds based on topological analysis of electron localization functions *Nature* **371** 683–6
[30] Henkelman G, Arnaldsson A and Jónsson H 2006 A fast and robust algorithm for Bader decomposition of charge density *Comput. Mater. Sci.* **36** 354–60
[31] Chang H, Wang H, Song K-K, Zhong M, Shi L-B and Qian P 2022 Origin of phonon-limited mobility in two-dimensional metal dichalcogenides *J. Phys. Condens. Matter* **34** 13003
[32] Su Y, Cao S, Shi L-B and Qian P 2021 Investigation of biaxial strain behavior and phonon-limited mobility for γ graphyne: First-principles calculation *J. Appl. Phys.* **130** 195703
[33] Jia Y, Zhao M, Gou G, Zeng X C and Li J 2019 Niobium oxide dihalides $NbOX_2$: a new family of two-dimensional van der Waals layered materials with intrinsic ferroelectricity and antiferroelectricity *Nanoscale Horizons.* **4** 1113–23
[34] Beck J and Kusterer C 2006 Crystal structure of $NbOBr_2$ *Zeitschrift Für Anorg. Und Allg. Chem.* **632** 2193–4
[35] Rijnsdorp J and Jellinek F 1978 The crystal structure of niobium oxide diiodide NbOI2 *J. Less Common Met.* **61** 79–82
[36] Wang W, Dai S, Li X, Yang J, Srolovitz D J and Zheng Q 2015 Measurement of the cleavage energy of graphite *Nat. Commun.* **6** 7853
[37] Shahrokhi M, Raybaud P and Le Bahers T 2020 On the understanding of the optoelectronic properties of S-doped MoO_3 and O-doped MoS_2 bulk systems: a DFT perspective *J. Mater. Chem. C* **8** 9064–74